AIMS Bioengineering, 2(4): 469-486.
DOI: 10.3934/bioeng.2015.4.469
Received date 12 August 2015,
Accepted date 25 October 2015,
Published date 29 October 2015

http://www.aimspress.com/

Research article

CMEIAS bioimage informatics that define the landscape ecology of immature microbial biofilms developed on plant rhizoplane surfaces

Frank B. Dazzo [1,*], Youssef G. Yanni [2], Ashley Jones [1], and Abdelgawad Y. Elsadany [2]

[1] Department of Microbiology & Molecular Genetics, Michigan State University, 567 Wilson Rd., East Lansing, Michigan 48824 USA
[2] Sakha Agricultural Research Station, Kafr El-Sheikh, 33717, Egypt

*** Correspondence:** E-mail: dazzo@msu.edu; Tel: +001-517-896-3986.

Abstract: Colonization of the rhizoplane habitat is an important activity that enables certain microorganisms to promote plant growth. Here we describe various types of computer-assisted microscopy that reveal important ecological insights of early microbial colonization behavior within biofilms on plant root surfaces grown in soil. Examples of the primary data are obtained by analysis of processed images of rhizoplane biofilm landscapes analyzed at single-cell resolution using the emerging technology of CMEIAS bioimage informatics software. Included are various quantitative analyses of the *in situ* biofilm landscape ecology of microbes during their pioneer colonization of white clover roots, and of a rhizobial biofertilizer strain colonized on rice roots where it significantly enhances the productivity of this important crop plant. The results show that spatial patterns of immature biofilms developed on rhizoplanes that interface rhizosphere soil are highly structured (rather than distributed randomly) when analyzed at the appropriate spatial scale, indicating that regionalized microbial cell-cell interactions and the local environment can significantly affect their cooperative and competitive colonization behaviors.

Keywords: bioimage informatics; CMEIAS; colonization behavior; computer-assisted microscopy; image analysis; rhizoplane; spatial ecology

1. Introduction

In contrast to the predominantly oligotrophic status of bulk soil, the rhizosphere soil surrounding roots and their rhizoplane epidermal surfaces are nutritionally enriched habitats

supported by exudation of plant photosynthates, resulting in biofilm colonization by zymogenous microorganisms that in turn, can significantly influence plant nutrition, health and disease, and therefore are important for sustainability of natural terrestrial ecosystems and agriculture [1].

Microscopy is the most direct way to examine microbial colonization of rhizoplane surfaces, but most often, that approach is only addressed qualitatively by presentation of "representative" micrographs of that landscape domain. The colonization intensity of the rhizoplane biofilm does not typically develop into a mature, confluent layer of microorganisms. Instead, its distribution of microcolony biofilms is discontinuous and spatially discrete, with an immature substratum coverage not typically exceeding 20% while the plant is still actively growing.

We have been developing a comprehensive suite of scientific software named Center for Microbial Ecology Image Analysis System (CMEIAS) to strengthen microscopy-based approaches that support microbial ecology research. Advancement of this emerging technology of bioimage informatics is driven by the need to fill major gaps using quantitative computational techniques to analyze microbes at spatial scales directly relevant to their ecophysiology, and obtain useful knowledge of their ecology *in situ* without cultivation. When fully developed and documented, each of these software applications is released for free download at our project website [2]. One of the CMEIAS modules features quantitative tools to analyze the landscape ecology of microorganisms during their growth within biofilms on biological and non-biological surfaces. Here we describe examples of bioimage informatics obtained by CMEIAS computer-assisted microscopy and digital image analysis of processed rhizoplane landscapes after their short-term growth in soil. These data reveal important insights of the *in situ* abundance and intensity of cell-cell interactions of microorganisms during their pioneer colonization of white clover seedling roots, and of a rhizobial biofertilizer strain on rice roots that significantly enhances the productivity of this major cereal crop.

2. Materials and Methods

2.1. Pioneer colonization of rhizoplane biofilms

White clover (*Trifolium repens* L. var. Dutch) seeds were planted 0.5 cm below the surface of a moistened sandy loam soil located at the Long-Term Ecological Research farm at the Michigan State University Kellogg Biological Station. Two day old seedlings were gently excavated and processed using an optimized protocol to dislodge rhizosphere soil from roots without obvious damage to the root hairs so that > 80% of the rhizoplane can be visualized by microscopy [3]. Processed seedling roots were stained with acridine orange (AO, 1:10,000 in 1% sodium pyrophosphate, NaPPi) for 1 minute, then washed with NaPPi, transferred to slides, mounted in 1:1 v:v NaPPi solution plus Vectashield photobleaching retardant, covered with a coverslip and examined by laser scanning confocal microscopy [4] (Meridian Instruments InFight microscope, 63x objective [1.6 NA], argon laser, 488 nm excitation/500–530 emission). Microbial biovolume was calculated using the CMEIAS Formula #2 with 98.4% accuracy [5], and their biomass carbon was calculated by the allometric scaling conversion of microbial biovolume (μm^3) to biomass C (fg) using the formula: $218 \times \text{biovolume}^{0.86}$ [5,6].

2.2. Colonization of rice rhizoplanes by a rhizobial biofertilizer strain

Rice (*Oryza sativa*) variety Giza 177 seeds were germinated and grown for 20 days in a clay loam soil (pH 7.29, 2.31% organic matter, 53.47 meq/100 g cation exchange capacity, 43.8:10.74:487.05 N: P:K) used for rice cultivation in the Kafr El-Sheikh governorate within the Egypt Nile delta. Washed roots were examined by indirect immunofluorescence microscopy using an antiserum specific for *Rhizobium leguminosarum* bv. trifolii strain E11 [7,8], and images were acquired by epifluorescence photomicrography (Ilford XP2 400 color film). This strain was isolated from surface-sterilized roots of rice grown in the Nile delta and is a biofertilizer inoculant that promotes rice growth and grain production under agronomic field conditions [9–11]. The local density of individual, brightly immunofluorescent cells was assessed within 30–35 quadrat transects (each microscope field was 440 μm in length) along the elongating axis of the replicated seedling rootlets.

2.3. Image analysis and statistics

Images were segmented, thresholded and analyzed using CMEIAS software [5,8,12–16]. Extracted data were statistically analyzed using EcoStat [17], Ecological Methodology [18], PAST [19], StatistiXL [20] and GS+ [21] software.

3. Results and Discussion

3.1. Pioneer rhizobacterial colonization

Figure 1A is an 8-bit grayscale image of a confocal optisectioned landscape area of the white clover rhizoplane after 2 days of growth in soil, with resolution of individual, AO-stained fluorescent bacteria. Figure 1B is its accurately segmented, thresholded derivative that was analyzed by various CMEIAS attributes of microbial abundance and spatial pattern of their distribution to obtain the data providing insights on their colonization behavior within the rhizoplane biofilm.

Various CMEIAS-extracted metrics that indicate the spatial abundance of all 135 fluorescent bacteria in Figure 1 are provided in Table 1. The magnitude of these metric values can be used to compare the size of the standing crop of microbial populations and communities *in situ* within biofilm landscapes [5,22,23]. They also provide significant insights on several ecologically relevant activities that drive biological diversity, including cell-cell interactions impacting on their colonization behavior, allometric scaling relationships between individual body size and metabolic activities, recent status of nutrient resource concentrations / apportionment / acquisition efficiency, intensity of predator-prey interactions, coexistence among neighbors competing for the same limited resources, community dominance-rarity relationships, productivity related to food web dynamics, and starvation stress physiology [5,16,23–28].

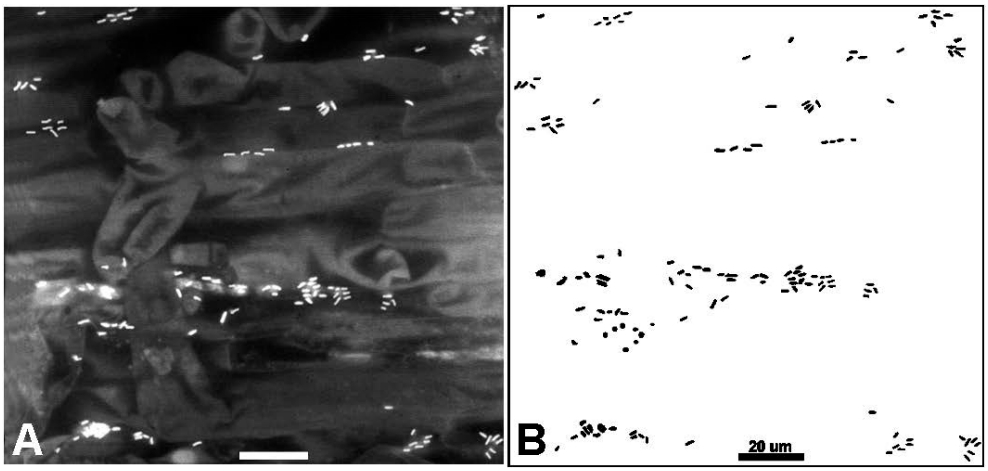

Figure 1. (A) Laser scanning confocal micrograph of an optisectioned rhizoplane landscape and associated microbial biofilm developed on a white clover seedling root grown in soil. Bar scale is 20.0 μm. (B) Segmented, binary derivative of Figure 1A that was thresholded to 100 grayscale brightness for image analysis.

Table 1. Spatial abundance of microorganisms computed by CMEIAS image analysis of the immature biofilm developed on the white clover rhizoplane (Figure 1).

Microbial Abundance Metric	Attribute Value
Image Area Analyzed (μm^2)	21,666.7
Cell Count	135
Spatial Density (cells/mm^2)	6,231
Cumulative Biovolume (μm^3)	211.1
Biovolume Intensity (um^3 / mm^2)	4,573,840.37
Cumulative Biomass C (ng)	42.22
Biomass C Intensity (ng C/mm^2)	1,948.45
Cumulative Biosurface Area (μm^2)	1,028.47
Biosurface Area Intensity (μm^2/mm^2)	47,467.12
Substratum Coverage (%)	1.21

The dependence of spatially structured heterogeneity on ecosystem function [28] provides the impetus to include spatial pattern analysis and landscape ecology in studies of microbial biofilms [23,29,30]. *In situ* spatial pattern analysis of microbes within biofilms reveals statistically defendable models indicating that their colonization behavior involves a spatially explicit process rather than occur independent of their location in this habitat [23,31]. Spatial dependence is positive

when neighboring organisms aggregate due to cooperative interactions promoting their growth, and is negative when conflicting/inhibitory interactions result in their uniform, self-avoiding colonization behavior [23,31,32]. The protocol to measure these distinctions of spatial proximity typically involves a sequence of initial statistical tests of the null hypothesis of complete spatial randomness, followed by additional quantitative measures of spatial dispersion/aggregation, and finally by powerful geostatistical analyses that model the spatial autocorrelation among neighboring pairs of organisms to define the *in situ* radial distances at which they interact with each other, plus produce interpolation maps of the intensities of those measured activities over the entire spatial domain, even at locations not sampled [23,29,31].

CMEIAS can extract various data from landscape images to perform these 3 major types of spatial pattern analyses that distinguish positive (aggregated), random (neutral) and uniform (negative) interactions [23,29,31]. The first is a plot-less point pattern analysis of nearest neighboring objects derived from measurement of distances between their object centroids. The second performs plot-based measurements of spatially explicit characteristics within contiguous quadrats defined by an optimized grid-lattice overlay of the landscape image. The third type of analysis explores the variation and connectivity in continuously distributed "Z-variate" attributes measured at georeferenced X, Y coordinate locations of sampling points within a landscape domain.

Several point pattern analyses of microbial distribution show a preponderance of aggregated spatial patterns and minor proportions of random plus uniform patterns in the rhizoplane biofilm landscape (Figure 1A). 87.4% of the 1st *vs.* 2nd nearest neighbor distances (Figure 2A) for all 135 microbes in the landscape area form a tight cluster within the 1st quartile of the full range, consistent with the majority having a clustered pattern over the entire domain. The empirical cumulative distribution function of the ranked plot of the 1st nearest neighbor distances (Figure 2B) is dominated by aggregated patterns of cells based on the position of their data points above the diagonal random trendline.

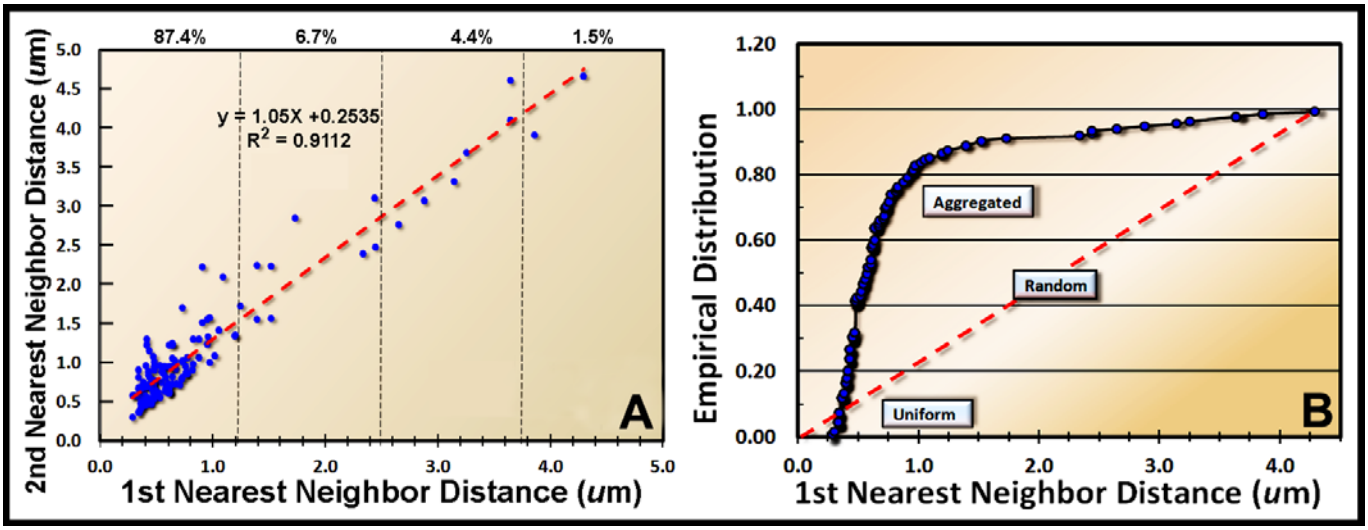

Figure 2. Point pattern analyses of pioneer rhizobacterial colonization. (A) 2-d scatterplot of 1st vs. 2nd nearest neighbor distances, with % proportions in each quartile. (B) Empirical cumulative distribution function of the 1st nearest neighbor distance.

Ripley's [33] multi-distance spatial cluster analysis is a useful sequel to the empirical cumulative distribution function and tests if the point pattern characteristics change with distance of the spatial scale of analysis. It plots the average point density as a function of distance from every object centroid within the landscape, indicating if the object at the specified distance is clustered, over-dispersed or enclosed within a simulated envelope of random distribution at multiple distances [19,33]. The results (Figure 3) indicate multimodal patterns, with 54.6% of the data points indicating clustered patterns above the random 95% confidence envelope, 13.1% within the simulated random confidence envelope, and 32.3% below the confidence envelope indicating their uniform patterns.

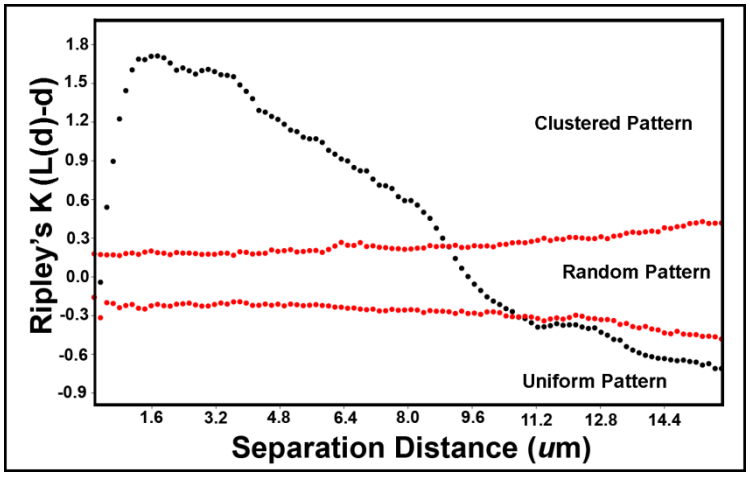

Figure 3. Ripley's K spatial pattern analysis of the microbes in the rhizoplane biofilm landscape image (Figure 1B). Donnelly edge-corrected Ripley's K (L(d)-d) points (black dots) and the simulated 95% confidence envelope of spatial randomness (red dots) are indicated.

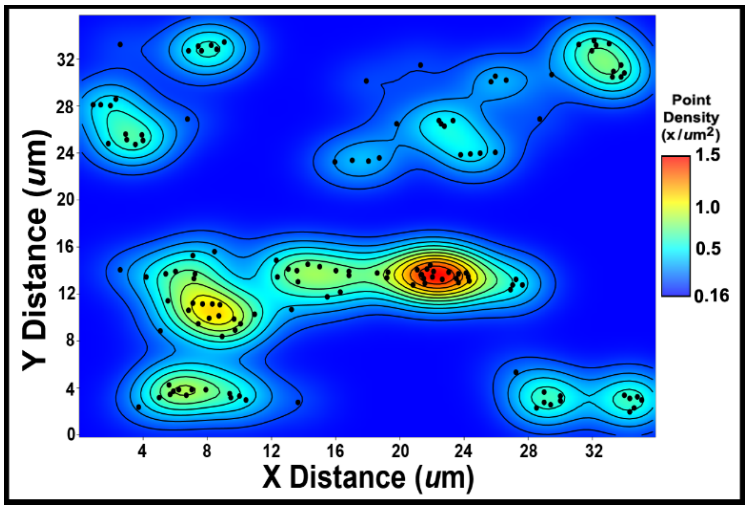

Figure 4. Smooth 2-d map of the kernel density of pioneer microbes in the rhizoplane biofilm landscape. The pseudocolored isopleth scaling identifies the clustered cell aggregates by providing an estimate of the number of microbes per local neighboring area.

Point pattern data can also be evaluated by statistical inference tests for complete spatial randomness and by plots that address the local density and directionality of microbial patterns within the biofilm landscape. Significant spatial aggregation was indicated by the Holgate's test with an A value of 0.553 (A > 0.5; $p < 0.05$), and by the Clarke and Evans Z value of −9.22 (Z < 1.96; $p < 2.86 \times 10^{-20}$). The local positioning of aggregated microbial cells creating microcolony biofilms is revealed by a 2-d kernel plot of point density clusters within the biofilm (Figure 4).

Further point pattern analyses address the angular positioning of these rod-shaped bacteria in the rhizoplane biofilm. The circular map (Figure 5A) shows the dominant, near-horizontal (0°) angular alignments of the microbial cells' major axis angle relative to the elongating axis of the rhizoplane landscape image. The corresponding Rayleigh's angular positioning test statistic of circular-uniform distribution computes a strong mean resultant vector Z value of 92.0 with an associated probability of 8×10^{-10} that this angular alignment is due to chance; therefore it cannot be dismissed as trivial or random. Further support of the ecological relevance of a preferential alignment of cells is provided by a 2-d directional plot that uses a continuous sector method [34] to identify linear point alignments. That plot reveals 33 point alignments that are dominated by near-horizontal configuration and whose angular orientations generate 28 intersecting "hot spot" epicenters of interpoint interactions (Figure 5B). Detailed inspection of the rhizoplane biofilm landscape image (Figure 1) corroborates this *in situ* colonization behavior by revealing the strong congregation of closely neighboring, sessile bacteria whose angular orientation is near-horizontal, aligned within the interepidermal grooved junctions of the elongating axis between adjacent epidermal cells where roots preferentially exude nutrients. (Note: the Figure 1 image is rotated 90° to conveniently fit on the printed page. The above discussion relates to the real vertical orientations of the interepidermal junctions of the rhizoplane on the geotropically growing root.)

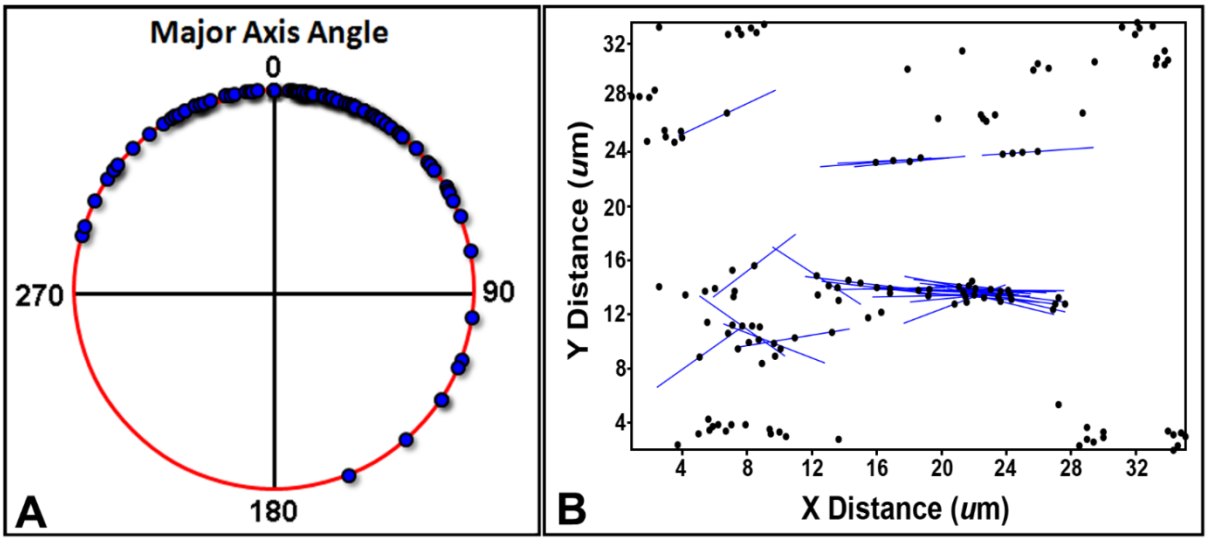

Figure 5. Angular positioning analyses of individual bacteria within the landscape image of the white clover rhizoplane biofilm. (A) Circular map indicating the angular orientation of individual bacteria. (B) Linear point alignments of the microbial cells showing numerous localized epicenters of clustered colonization behavior.

The CMEIAS Quadrat Maker is a computing tool designed to alleviate the important but cumbersome, time-consuming tasks of optimizing the dimensions of the grid-lattice overlay of landscape images and producing the individual quadrat image derivatives for plot-based spatial distribution analysis of the landscape domain [14]. These quadrat-based analyses are designed to examine how spatial patterns of the organisms of interest vary with the scale at which they are measured. Figure 6 shows the graphical user interface of CMEIAS Quadrat Maker, with the optimally gridded 7 × 4 index image of the pioneer rhizobacteria on the rhizoplane landscape and column-row annotation of the contiguous quadrats that cover the entire spatial domain. Figure 7 is a 3-d surface plot of the discontinuous distribution of microbial biovolume allocated to each quadrat.

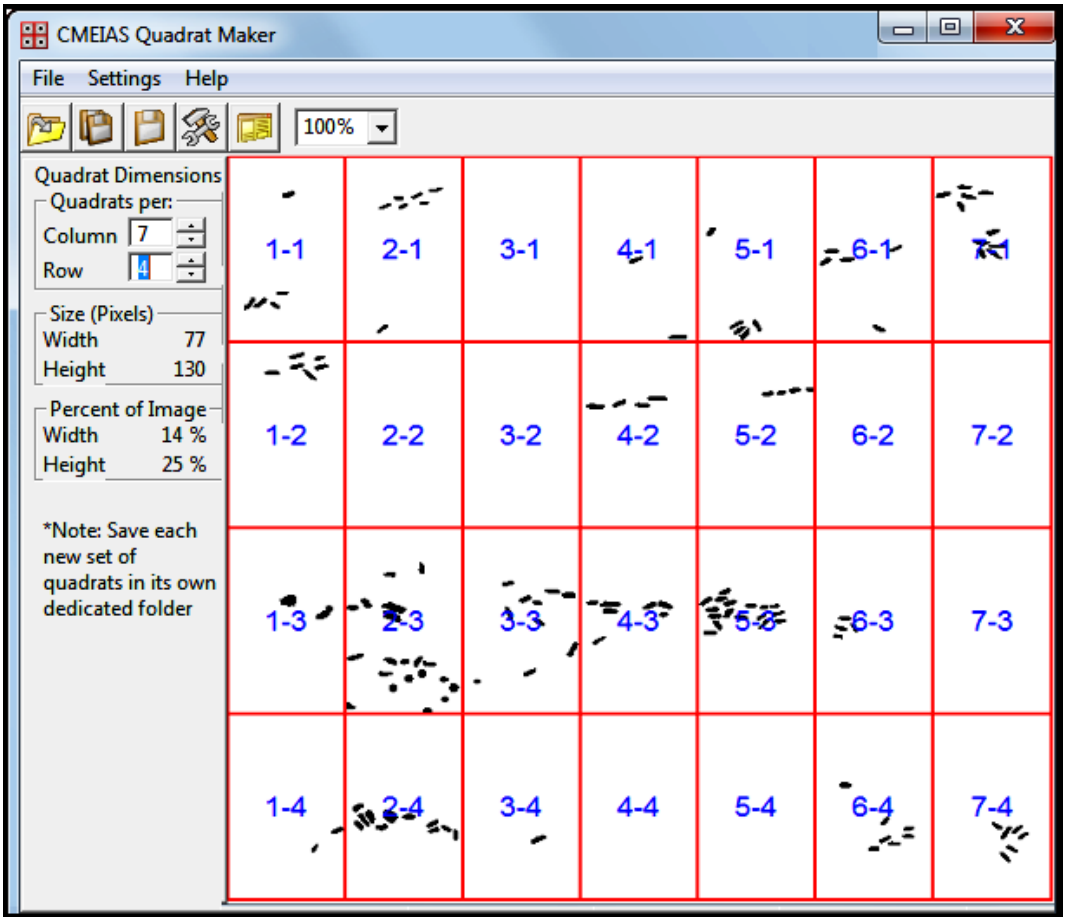

Figure 6. Graphical user interface of the CMEIAS Quadrat Maker software and the segmented rhizoplane landscape image of pioneer rhizobacteria (From Figure 1B) overlaid with the optimized quadrat grid-lattice raster that is annotated to indicate each quadrat's column-row location.

Several plot-based metrics use the distribution of cell abundance within the array of quadrat counts from the landscape image to compute indices of dispersion that distinguish aggregated *vs*. random *vs*. uniform spatial pattern distributions. Table 2 presents 3 commonly used spatial pattern indices derived from the quadrat-based abundance data of the pioneer rhizoplane biofilm developed on the white clover rhizoplane. Each test result indicates that the spatial pattern of distribution for the rhizobacteria is aggregated, consistent with the point pattern spatial analyses of the same landscape.

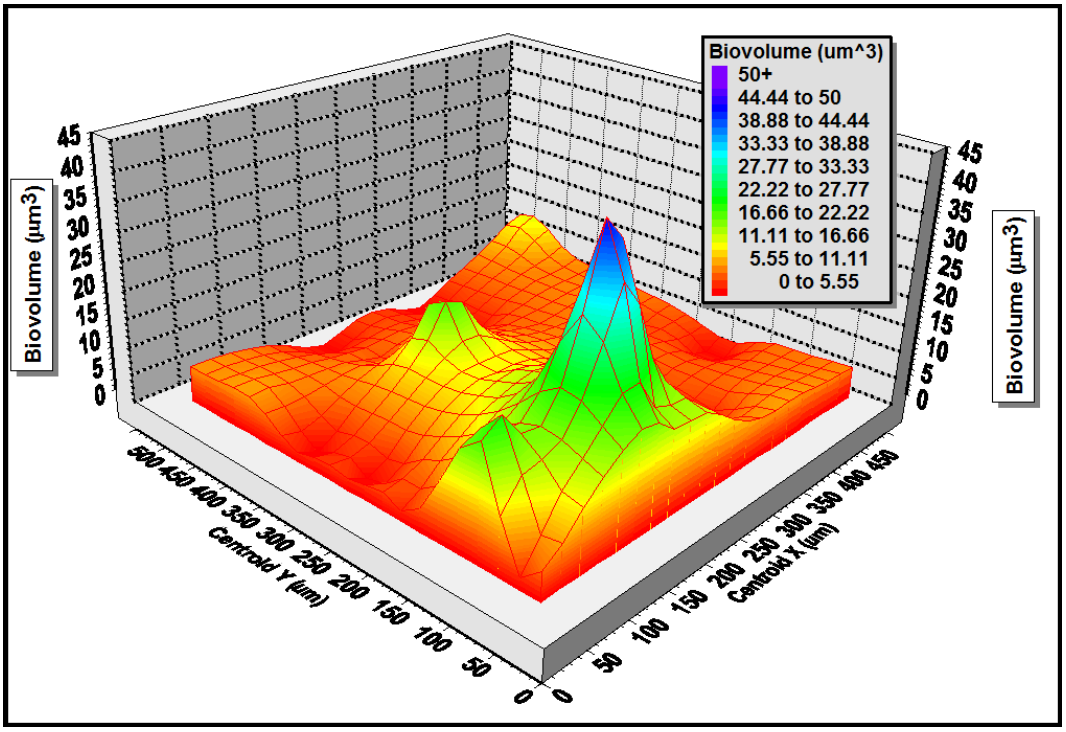

Figure 7. 3-dimensional surface plot of the microbial biovolume distribution in the grid raster of the rhizoplane biofilm (Figure 6). Quadrats are georeferenced based on their object-weighted X, Y Cartesian coordinates relative to the 0, 0 landmark origin located at the bottom center corner.

Table 2. Spatial analysis of cell dispersion based on the abundance of pioneer microbial cells in contiguous quadrats of the rhizoplane landscape analyzed by CMEIAS.

Quadrat-Based Index	Index Value	Spatial Pattern
V/M Index of Dispersion	4.689 (p = 0.001)	aggregated (> 1)
Morisita Index of Dispersion	1.889	aggregated (> 1)
Standardized Morisita Index	0.5139	aggregated (> 0)

The geostatistical method of spatial pattern analysis measures the degree of dependency among observations in a geographic space to evaluate the continuity or continuous variation of spatial patterns over that entire domain [35]. It quantifies the resemblance between neighbors as a function of spatial separation distance [35]. Data are autocorrelated when nearby neighbor pairs are more similar than far neighbor pairs, as is the case in aggregated distributions [36]. When found, autocorrelation results can be mathematically modeled to connect various spatially dependent relationships derived from regionalized variable theory and also make optimal, statistically rigorous interpolation (kriging) maps of the parameter at unmeasured locations within that spatial domain, based on analysis of its weighted average from neighboring sampled locations [35].

We developed a CMEIAS Cluster Index as an ideal geostatistical “Z-variate” metric that sizes the intensity of aggregated colonization behavior commonly occurring among neighboring cells

during microbial biofilm development [7,23,29,31]. CMEIAS computes this index as the inverse of the separation distance between the object centroid of each bacterial cell and its 1st nearest cell neighbor [7]. Figure 8A shows the quartile sample posting of the bin range of the Cluster Index for each bacterial cell *in situ* within the landscape image of the pioneer rhizoplane biofilm. Figure 8B is a plot of the Moran's Intensity index for the spatially autocorrelated Z variate relationship between paired observations among neighboring cells in the landscape image. The result indicates both positive (cooperative) and negative (conflicting) autocorrelated interactions between neighboring cells that affect their aggregation behavior over the 60 μm range of separation distances examined. The cumulative sum of Moran's I value is positive (Figure 8B), indicating that cooperative spatial aggregation is the dominant pattern/behavior that exceeds what would be expected if random within the examined geographic space, which is consistent with the point pattern and quadrat-based results.

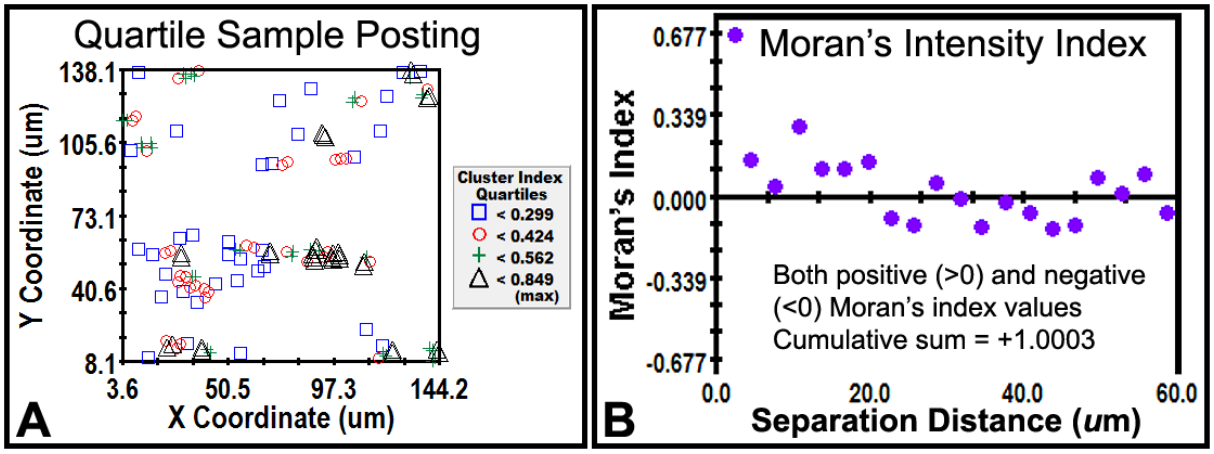

Figure 8. Quartile sample posting (A) and Moran's Index (B) of the intensity of the CMEIAS Cluster Index for the bacteria within the pioneer rhizoplane biofilm.

At the center of the geostatistical analysis is the semivariogram plot, which defines the extent to which the measured Z-variate (e.g., intensity of cell aggregation pattern) exhibits autocorrelated spatial dependence between pairs of sampled locations [35]. Geostatistical analysis of the CMEIAS cluster index for the microbes in the pioneer rhizoplane biofilm produced the semivariogram mathematical model shown in Figure 9. The high coefficient of determination (r^2; 0.865) and low residual sum of squares (2.397×10^{-4}) indicate a good fit of the spherical isotropic variogram model to the geostatistical data showing significant spatial autocorrelation of the microbes' clustered colonization behavior. The nugget value (Y intercept of 0.00250 at X = 0 separation distance) indicates the very low amount of measured microstructure that is not spatially dependent over the separation range examined. Its small value also indicates that the sampling points are sufficient in quantity and are sampled at the proper spatial scale for the geostatistical analysis. Also indicated in Figure 9 (green arrow) is the effective separation range (the X-axis intercept at 95% of the asymptote height). This metric defines the maximal separation distance between sampling points at which the Z variate is autocorrelated. In this example, the effective separation range extends out from individual cells to a distance of 22.0 μm, representing the *in situ*, real-world distance at which bacterial cells influence their neighbor's ability to congregate locally within the defined spatial domain. CMEIAS object analysis indicates that the furthest 1st nearest neighbor distance for the bacteria in the pioneer

biofilm landscape is 4.3 μm, thus they are positioned well within the 22.0 μm effective separation range of influence. Also, this distance of interaction is sufficiently extended to include the cluster-to-cluster microcolony biofilm interactions *in situ*. Ecophysiological processes resulting in this type of positive autocorrelation would, *inter alia*, include nutritional cross-feeding, elaboration of signal molecules that activate genes positively affecting cell growth into microcolonies, localized detoxification/degradation of extracellular metabolic wastes, and refuge from predatory activity [23].

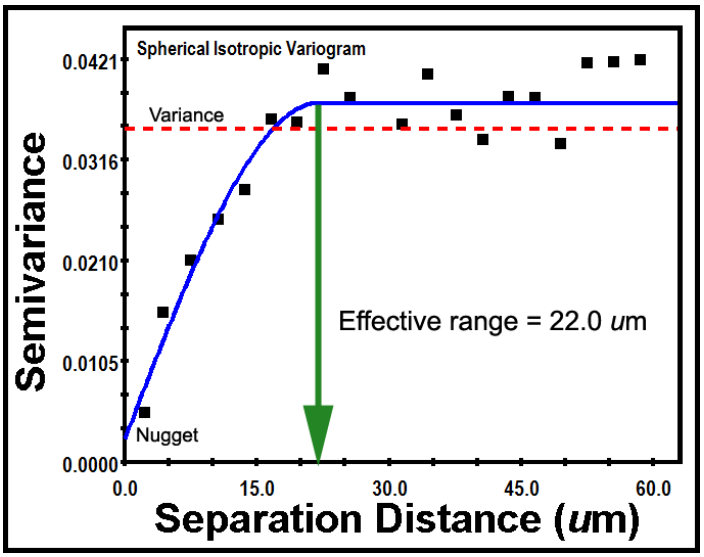

Figure 9. Geostatistical semivariogram of the spatially autocorrelated Cluster index for the pioneer rhizobacteria colonizing the white clover rhizoplane biofilm. Effective range is 22.0 μm.

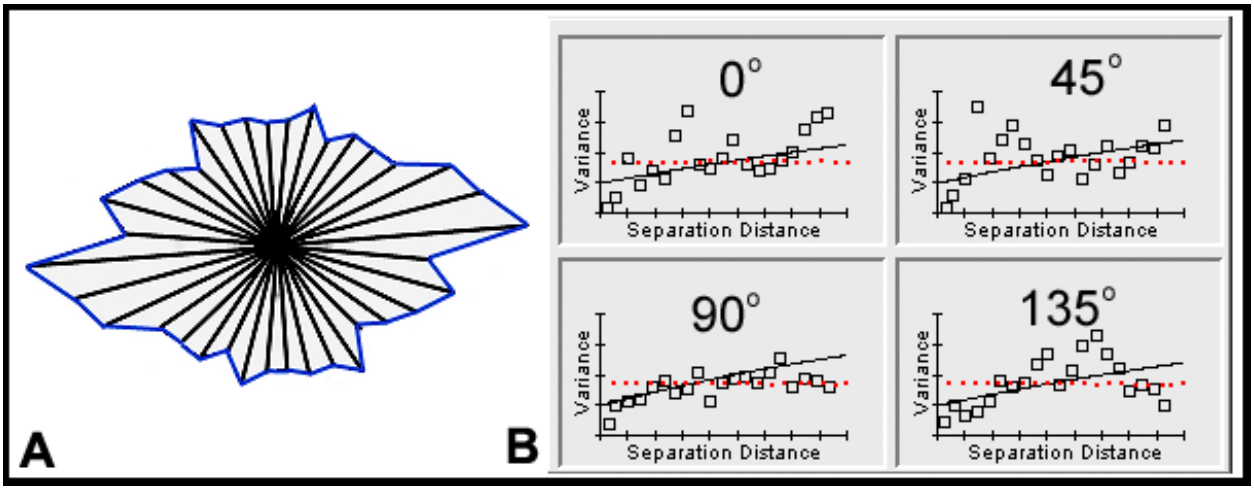

Figure 10. Detection of anisotropy in the spatial pattern of pioneer rhizobacteria colonized in the pioneer biofilm on the rhizoplane landscape. (A) Rose plot of foreground object mean intercept lengths with an aspect ratio >1.000. (B) Semivariograms of cluster index autocorrelation with varying effective ranges measured at four different compass directions.

Geostatistics can detect patches of organisms whose patterns of distribution have significant departure from the null hypothesis of isotropy, and instead have anisotropic spatial autocorrelation in patterns of directionally dependent intensities at certain compass directions. This occurs sometimes during biofilm formation on rhizoplanes where the bacteria selectively partition into local microenvironments favored by increased availability of nutrient resources located between adjacent cylindrical epidermal cells oriented parallel to the longitudinal axis of the root as described earlier. A few clusters of bacteria have anisotropic alignment in Figure 1 (also see Figure 5). This anisotropy is indicated in the rose plot (Figure 10A) where the radial lines of the mean intercept length of foreground object pixels vary in length, producing a polygon with aspect ratio greater than 1.000. In this case, lines of bacterial cell intercepts have greater lengths in the horizontal orientation, with an aspect ratio of 2.232. Geostatistical anisotropy is also indicated when the effective separation range changes significantly in semivariograms plotted in different compass directions (Figure 10B).

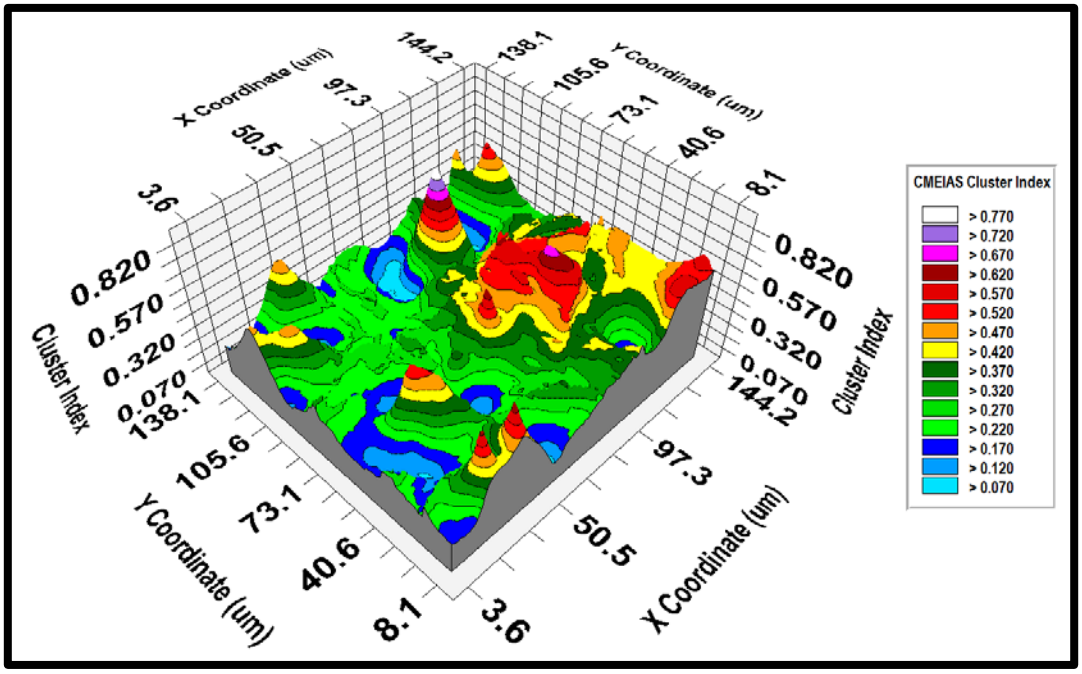

Figure 11. Three-dimensional kriging map of the spatially autocorrelated, clustered colonization behavior of the pioneer rhizobacteria within the rhizoplane biofilm landscape of white clover. The Z-variate parameter used in this geostatistical analysis is the CMEIAS cluster index.

After computing the best-fit geostatistical autocorrelation model, a kriging map can be built to indicate a continuous interpolation of the spatial variability in intensity of the Z-variate parameter within the entire spatial domain, even in areas not physically sampled. The map's isopleth contour lines connect points of equal Z-variate values, and the pseudocolored scale reveals the relative gradient of its intensity. The 3-dimensional kriging map of Figure 11 shows the intense peaks and valleys of clustered colonization behavior associated with the pioneer rhizobacterial biofilm on the clover rhizoplane landscape. Such geostatistical methods have been used in previous CMEIAS-based studies that predict the *in situ* diffusion gradients of extracellular signal molecules that influence/mediate these positive, cooperative cell-to-cell interactions within biofilms developed on

roots [1,23,29,30].

Biofilm landscapes commonly have complex architectures that exhibit self-similar fractal geometry when measured at different spatial scales [15,37–39]. Fractal dimension values greater than 1.000 for this self-similarity metric arise from the scale-dependent heterogeneous fractal variability in limiting resource partitioning, and reflect the high efficiency at which organisms cooperatively position themselves spatially and physiologically when faced with the interactive forces of coexistence to optimize their allocation of nutrient resources on a local scale [40]. Various ecological studies suggest that metabolic processes used for growth physiology rely on the hierarchical fractal-like nature of resource distribution networks, and that organisms have exploited a fourth spatial dimension by evolving hierarchical fractal-like structured spatial distributions designed to maximize nutrient resource acquisition and allocation [40–42]. We will soon release CMEIAS JFrad software featuring a unique combination of algorithms to compute fractal dimension of foreground object coastlines, enabling the user to discriminate the fractal geometry of microbial biofilm architectures at both microcolony and single-cell resolutions [15]. JFrad analysis of the rhizoplane landscape in Figure 1 indicates that the spatial pattern of the pioneer rhizobacteria has positive fractal geometry, with fractal dimensions of 1.104, 1.144, and 1.798 obtained using the computational methods of Eucledian distance map, dilation and parallel lines, respectively.

3.2. Colonization of rice roots by indigenous populations of rhizobia

We have described a natural, plant growth-promoting association between selected strains of *Rhizobium leguminosarum* bv. trifolii and rice roots, and our translational studies have shown that this plant-microbe interaction can be exploited by biofertilization technologies that use selected strains to enhance rice production under real-world agroecosystems [9–11,29]. An important autecological topic currently under investigation is the extent that the indigenous population of a key inoculant strain is able to colonize the rice rhizoplane biofilm while significantly enhancing the productivity of this very important cereal crop. Our approach has been to use computer-assisted microscopy to quantify the *in situ* colonization intensity of the rhizobial strain of interest within the rhizoplane biofilm developed when the roots are grown in soils used for rice production.

Figure 12 shows a portion of the rice rhizoplane landscape containing the rhizobial biofertilizer strain detected by immunofluorescence microscopy using a strain-specific antibody, and a matrix plot of the rhizoplane colonization intensity by this strain in contiguous 440 μm-long quadrat transects along the elongating axis of 3 replicated rice rootlets grown in soil. The variation in colonization intensities is noteworthy. This patchy pattern likely reflects a combination of the discontinuous distribution of local indigenous population densities that encounter the root as it grows geotropically into deeper regions within the soil, and the cooperative behavior of attached cells that grow into rhizoplane microcolony biofilms *in situ*. This result emphasizes the importance of measuring the distribution of microbes on roots at the appropriate micrometer spatial scales that are directly relevant to the niches they occupy at the rhizoplane/rhizosphere soil interface.

The various quantitative indices of dispersion indicated in Table 2 can be used to compute the overall spatial pattern for these quadrat-based data. Another method, called the “two-term local quadrat variance” (TTLQV), can also be used to analyze the spatial pattern of this 1-dimensional transect of indigenous population intensity of the target strain on the rhizoplane biofilm. TTLQV is an optimal choice because it does not lose spatial information derived from the relative positions of

the quadrat sampling units [43]. It involves a sampling of contiguous quadrat units of equal size spanning a linear transect that can then be combined into larger blocks to evaluate spatial patterns of local densities at multiple spatial scales [18,43,44]. The intensity data are evaluated by plotting the variance in intensity along the transect against a range of contiguous quadrat block sizes of the transect. Patterns of distribution are aggregated when distinct peaks are indicated at a block size equivalent to the radius of the microcolony area, random when the data fluctuate irregularly with no pattern, and uniform when the variances are low and do not fluctuate with block size [18].

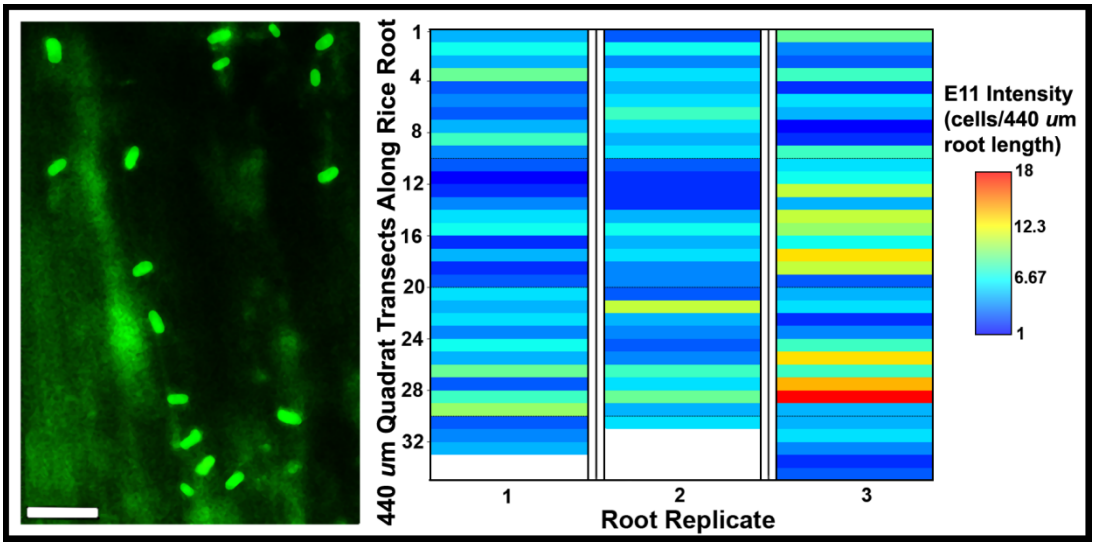

Figure 12. Colonization of rice roots by indigenous populations of *R. leguminosarum* bv. trifolii biofertilizer strain E11 in soil. Left: detection of individual cells in the rhizoplane biofilm by immunofluorescence microscoy (epifluorescence, 24-bit color photomicrograph). Bar scale is 10 μm. Right: matrix plot of colonization intensity by indigenous populations of E11 in rhizoplane biofilms on 3 rice rootlets.

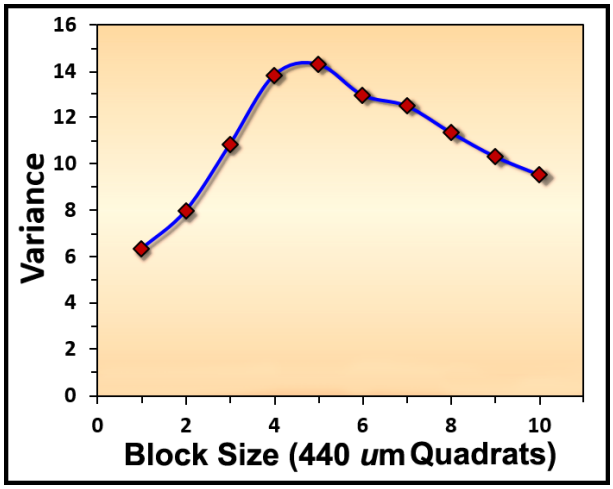

Figure 13. TTLQV plot indicating an aggregated pattern of colonization intensity of indigenous populations of *R. leguminosarum* bv. trifolii strain E11 along transects of rice rootlets grown in soil.

Figure 13 shows an example of this TTLQV analysis applied to the quadrat counts for the positive immunofluorescent cells along the elongating axis of the rice rootlet. The peak at a block size of 4–5 quadrat lengths indicates that aggregates of greatest E11 colonization intensity are separated from each other on the rootlets by an average distance of 3.52–4.40 mm (*i.e.*, twice the peak block size).

4. Conclusions

Colonization of the rhizoplane habitat is an important activity that enables certain microorganisms to promote plant growth. In this paper, we describe various applications of computer-assisted microscopy using CMEIAS bioimage informatics software to reveal important ecological insights of early microbial colonization behavior within biofilms developed on root surfaces grown in soil. These quantitative analyses of *in situ* microbial colonization behavior are optimally performed with images of immature biofilms acquired at single-cell resolution, during early seral stages of development before microcolony biofilms become 3-dimensional and approach their mature climax coverage of the substratum (typically ≤ 20% on the rhizoplane). Included are various quantitative analyses of the *in situ* landscape ecology of microbes during their pioneer colonization of white clover roots, and of a rhizobial biofertilizer strain colonized on rice roots while it significantly enhances the productivity of this crop plant. The results show that spatial patterns of immature microcolony biofilms developing on rhizoplanes that interface rhizosphere soil are highly structured and *symphonic* (rather than distributed randomly) when analyzed at the appropriate spatial scale, indicating that regionalized microbial cell-cell interactions and the local environment can significantly affect their cooperative and competitive colonization behaviors. This emerging technology of CMEIAS bioimage informatics provides several analytical tools to explore the landscape ecology and bioengineering applications of natural and managed microbial biofilms.

Acknowledgments

Portions of the work reported here were supported by the United States-Egypt Science & Technology Development Fund (Projects ID3852 and 58-3148-1-140), Michigan State University Kellogg Biological Station Long-Term Ecological Research program (NSF DEB 1027253), and Michigan AgBioResearch.

Conflict of Interest

All authors declare no conflict of interest concerning this paper.

References

1. Dazzo FB, Gantner S (2012) Rhizosphere. *In*: Schmidt T, Schaechter M, *Topics in Ecological and Environmental Microbiology,* Massachusetts, USA*:* Elsevier Press, 467–479.
2. Dazzo FB, McGarrell D (2015) CMEIAS Center for Microbial Ecology Image Analysis System. Available from: http://cme.msu.edu/cmeias/.
3. Dazzo FB (2006) COST 631: Visualization of the rhizoplane microflora by computer-assisted microscopy and spatial analysis by CMEIAS image analysis. In: Luster J., Finlay R., *Handbook*

of Methods Used in Rhizosphere Research, Section 4.1, Birmensdorf, Swiss Federal Research Institute.

4. Dazzo FB, Mateos P, Orgambide G, et al. (1993) The infection process in the *Rhizobium*-legume symbiosis and visualization of rhizoplane microorganisms by laser scanning confocal microscopy. In: Guerrero R., Pedros-Alio C., *Trends in Microbial Ecology,* Barcelona, Spain: Spanish Society for Microbiology, 259–262.
5. Folland I, Trione D, Dazzo FB (2014) Accuracy of biovolume formulas for CMEIAS computer-assisted microscopy and body size analysis of morphologically diverse microbial populations and communities. *Microbial Ecology* 68: 596–610.
6. Loferer-Krobacher M, Klima J, Psenner R (1998) Determination of bacterial cell dry mass by transmission electron microscopy and densitometric image analysis. *Appl Environ Microbiol* 64: 688–694.
7. Dazzo FB, Joseph AR, Gomaa A, et al. (2003) Quantitative indices for the autecological biogeography of a *Rhizobium* endophyte of rice at macro and micro spatial scales. *Symbiosis* 35: 147–158.
8. Dazzo FB, Schmid M, Hartmann A (2007) Immunofluorescence microscopy and fluorescence *in situ* hybridization combined with CMEIAS and other image analysis tools for soil- and plant-associated microbial autecology. In: Garland J, Hurst C, Lipson D, et al., *Manual of Environmental Microbiology*, Vol 59, 3rd Ed, Washington DC, USA: American Society for Microbiology Press, 712–733.
9. Yanni YG, Rizk RY, Corish V, et al. (1997) Natural endophytic association between *Rhizobium leguminosarum* bv. trifolii and rice roots and assessment of its potential to promote rice growth. *Plant and Soil* 194: 99–114.
10. Yanni YG, Rizk RY, Abd El-Fattah FK, et al. (2001) The beneficial plant growth-promoting association of *Rhizobium leguminosarum* bv. trifolii with rice roots. *Austr J Plant Physiol* 28: 845–870.
11. Yanni YG, Dazzo FB (2010) Enhancement of rice production using endophytic strains of *Rhizobium leguminosarum* bv. trifolii in extensive field inoculation trials within the Egypt Nile delta. *Plant and Soil* 336: 129–142.
12. Liu J, Dazzo FB, Glagoleva O, et al. (2001) CMEIAS: a computer-aided system for the image analysis of bacterial morphotypes in microbial communities. *Microbial Ecology* 41: 173–194.
13. Gross, CA, Reddy C, Dazzo FB (2010) CMEIAS color segmentation: an improved computing technology to process color images for quantitative microbial ecology studies at single-cell resolution. *Microbial Ecology* 59: 400–414**.**
14. Dazzo F, Gross C (2012) CMEIAS Quadrat Maker: a digital software tool to optimize grid dimensions and produce quadrat images for landscape ecology spatial analysis. *J Ecosystem and Ecography* 3: 4 (136).
15. Ji Z, Card K, Dazzo FB (2015) CMEIAS JFrad: a new computing toolkit to discriminate the fractal geometry of landscape architecture and spatial patterns of individual cells in microbial biofilms. *Microbial Ecology* 69: 710–720.
16. Dazzo FB, Liu J, Gross C, et al. CMEIAS v3.10: Advanced Computational Tools of Image Analysis Software Designed to Strengthen Microscopy-Based Approaches for Understanding Microbial Ecology. All-Investigator Meeting Kellogg Biological Station Long-Term Ecological Research Mtg, 2015. Available from: http://lter.kbs.msu.edu/abstracts/493.

17. Towner H EcoStat: an Ecological Analysis Program, version 1.03. Exeter Software, Setauket, New York. 1999 available from: http://www.exetersoftware.com/cat/Trinity/ecostat.html.
18. Krebs C Ecological Methodology, version 7.2, Exeter Software, Setauket, NY, 2011, available from:http://www.exetersoftware.com/cat/ecometh/ecomethodology.html.
19. Hammer O, Harper DAT, Ryan PD (2001) PAST: Paleontological statistics software package for education and data analysis. *Palaeontol Electron* 4: 1–9.
20. Roberts A, Withers P. StatistiXL, Version 1.10. Broadway-Nedlands, Kalamunda, Australia, 2012, available from: http://www.statistixl.com/default.aspx.
21. Robertson GP GS+ Geostatistics, Version 9.0 Gamma Design Software, Plainwell, MI USA. 2004, Available from: http://www.gammadesign.com/default.aspx.
22. Paul EA, Harris D, Klug MJ, et al. (1999) The determination of microbial biomass. In: Robertson GP, Coleman DC, Bledsoe CS, et al., *Standard Soil Methods for Long-Term Ecological Research*. New York, USA: Oxford University Press, 291–317.
23. Dazzo FB, Klemmer KJ, Chandler R, et al. (2013) *In situ* ecophysiology of microbial biofilm communities analyzed by CMEIAS computer-assisted microscopy at single-cell resolution. *Diversity* 5: 426–460.
24. Petchey OI, Long ZT, Morin PJ (2007) The consequences of body size in model microbial ecosystems. In: Hildrew A, Raffelli D, Edmonds-Brown R, *Body Size: the Structure and Function of Aquatic Ecosystems*. Cambridge UK: Cambridge University Press, 245–265.
25. Magurran AE (2004) *Measuring Biological Diversity*. Malden Massachusetts, USA: Blackwell.
26. Gonzalez JM, Sherr EB, Sherr BF (1990) Size-selective grazing on bacteria by natural assemblages of estuarine flagellates and ciliates. *Appl Environ Microbiol* 56: 583–589.
27. Fukuda M, Matsuyama J, Katano T et al. (2006) Assessing primary and bacterial production rates in biofilms on pebbles in Ishite Stream, Japan. *Microbial Ecology* 52: 1–9.
28. Legendre P, Legendre L (2012) *Numerical Ecology*, 3rd Ed., Amsterdam The Netherlands: Elsevier.
29. Dazzo FB, Ganesan I, Yanni YG (2014) Spatial ecology of rhizobacterial colonization on roots analyzed by CMEIAS computer-assisted microscopy at single-cell resolution. In: Singh DP, Singh H, *Trends in Soil Microbial Ecology*, Chapter. 4, Houston USA: Studium Press, 67–92.
30. Gantner S, Schmid M, Dürr C, et al. (2006). *In situ* spatial scale of calling distances and population density-independent *N*-Acylhomoserine lactone mediated communication by rhizobacteria colonized on plant roots. *FEMS Microbiol Ecol* 56: 188–194.
31. Dazzo FB (2012) CMEIAS-aided microscopy of the spatial ecology of individual bacterial interactions involving cell-to-cell communication within biofilms. *Sensors* 12: 7047–7062.
32. Perry J (1998) Measures of spatial patterns for counts. *Ecology* 79: 1008–1017.
33. Ripley BD (1979) Tests of "randomness" for spatial point patterns. *J Roy Statist Soc B* 41: 368–374.
34. Hammer Ø (2009) New methods for the statistical detection of point alignments. *Computers and Geosciences* 35: 659–666.
35. Robertson GP (1987) Geostatistics in ecology: interpolating with known variance. *Ecology* 68: 744–748.
36. Ettema CH, Wardle DH (2002) Spatial soil ecology. *Trends in Ecology and Evolution* 17: 177–183.

37. Zahid W, Ganczarczyk J (1994) A technique for a characterization of RBC biofilm surface. *Water Res* 28: 2229–2231.
38. Hermanowicz S, Schindler U, Wilderer P (1995) Fractal structure of biofilms: new tools for investigation of morphology. *Water Sci Technol* 32: 99–105.
39. Yang X, Beyenal H, Harkin G, et al. (2000) Quantifying biofilm structure using image analysis. *J Microbiol Methods* 39: 109–119.
40. Ritchie ME (2010) *Scale, Heterogeneity, and the Structure and Diversity of Ecological Communities.* Princeton, NJ USA: Princeton University Press.
41. Sugihara G, May RM (1990) Applications of fractals in ecology. *TREE* 5: 79–86.
42. West G, Brown J, Enquist B (1999) The fourth dimension of life: fractal geometry and allometric scaling of organisms. *Science* 284**:** 1677–1679.
43. Dale MRT, Fortin MJ (2014) *Spatial Analysis: a Guide for Ecologists*. 2nd Ed. Cambridge UK: Cambridge University Press.
44. Hill MO (1973) The intensity of spatial pattern in plant communities. *J Ecol* 61: 225–235.

AIMS Press